Cancer Chemotherapy and Pharmacology (2019) 83:361–374
https://doi.org/10.1007/s00280-018-3735-0

ORIGINAL ARTICLE

Murine RAW264.7 cells as cellular drug delivery carriers for tumor therapy: a good idea?

Huangliang Zheng[1] · Jiaqi Li[1] · Xiang Luo[1] · Cong LI[1] · Ling Hu[1] · Qiujun Qiu[1] · Junqiang Ding[1] · Yanzhi Song[1] · Yihui Deng[1]

Received: 1 August 2018 / Accepted: 25 November 2018 / Published online: 30 November 2018

Abstract

Macrophage-mediated drug delivery system has emerged and gained wide interest as a novel strategy for cancer treatment. Among them, RAW264.7 cell was commonly used as the macrophage model for antitumor drug loading and delivery. However, this cell line was a macrophage-like cancerous cell with both immunogenicity and pro-tumorigenic properties, which may interfere with the positive response of the host immune system to developed tumor. Thus, the safety and efficacy of the RAW264.7 cell line as a drug carrier for cancer therapy remain questionable. Here, we constructed doxorubicin-loaded RAW264.7 cells and examined its antitumor efficacy in S180 tumor-bearing mice. The bio-distribution of RAW264.7 cells was determined by in vivo imaging technique, showing a high accumulation level of RAW264.7 cells in mice livers, spleens, and thymuses. A phenomenon of accelerated tumor growth was observed in mice treated with doxorubicin-loaded RAW264.7 cells. Thereafter, the effect of frequency, dose, and viability of injected RAW264.7 cells on S180 tumor growth was further investigated. The underlying mechanism was confirmed, attributing to the immune tolerance induced by excessive RAW264.7 cells. Our findings emphasized the latent limitation of RAW264.7 cells as drug carrier in current researches, and provided an experimental basis for the clinical safety of cell-mediated drug delivery system.

Keywords Cell-mediated drug delivery system · RAW264.7 cell · Immune tolerance · Doxorubicin

Introduction

The development of a tumor-targeting drug delivery system is one of the most crucial goals in the oncologic field to improve the therapeutic index of anticancer agents. Macrophage-mediated drug delivery systems have emerged as a promising strategy and gained wide interest for their ability to exhibit inflammatory chemotaxis and traverse biological barriers [1–3]. During tumor progression, monocytes are recruited from blood stream to tumor inflammatory area and differentiate into tumor-associated macrophages (TAMs) [4, 5], which promote tumor growth and constitute up to 80% of the total tumor mass [6]. Due to the pivotal role of macrophages in tumor development, drug-loaded macrophages acting as Trojan horses are an attractive choice for tumor therapy [7, 8].

✉ Yihui Deng
pharmdeng@gmail.com

[1] School of Pharmacy, Shenyang Pharmaceutical University, 103 Wenhua Road, Shenyang 110016, Liaoning, China

Despite great efforts in the development of macrophage-mediated drug delivery, there is as yet limited success [9]. Accumulation of drug-loaded macrophages in the liver has been found in several studies [10–12], which makes us think about the potential danger of these improperly used allogenic cellular carriers. Among them, the mouse macrophage-like cell line, RAW264.7, is commonly used due to its accessibility [11–14]. However, RAW264.7 cells were first introduced by Raschke et al. in 1978 as macrophage-like cancer cells established from murine tumors [15], possessing both the immunogenicity and pro-tumorigenic property. Thus, the safety and efficacy of the RAW264.7 cell line as a drug carrier for the tumor treatment remain unexplored.

For cell allograft, several clinical studies have reported adverse immune responses following allogenic cells transfusion, such as acute graft-versus-host disease (GVHD) [16], and cytokine release syndrome (CRS) in artificially processed chimeric antigen receptor T (CAR-T) cell therapy [17, 18]. Moreover, other clinical data have indicated that an immune tolerance could be established by allogenic cell transplantation as a fundamental immune regulation to

maintain the homeostasis of the host [19, 20], which was predominately mediated by regulatory *T* cells (T_{reg}) [21, 22].

Importantly, immune tolerance following allogenic transplantation can interdict the virtuous cancer-immunity cycle [23], thus, contributing to the deterioration and metastasis of tumor [24]. Early data have suggested that the relative risk of de novo malignancies in patients who have received successful liver transplants is unexpectedly increased [25]. Furthermore, an elegant study by Curiel et al. revealed that homeostatic peripheral tolerance might result in the growth of human tumors in vivo [26]. Therefore, the correlation between drug delivery strategies using allogenic RAW264.7 cells and the development of immune tolerance needs to be clarified.

In the current study, we constructed DOX-loaded RAW264.7 cells and demonstrated an immune tolerance induced by these allogenic cells, resulting in the promotion of growth of murine S180 tumor with an obvious dose dependency. These results highlighted the inappropriate use of RAW264.7 cells as drug carriers and showed a need for more studies focusing on the interactions of transplanted cells with the recipient immune system in cell-mediated drug delivery research.

Materials and methods

Materials

Doxorubicin hydrochloride salt (DOX) was sourced from Beijing HuaFeng Co., Ltd. (Beijing, China). Rapamycin was acquired from Taizhou Hongyao Chemical Co., Ltd. (Taizhou, China). *N*-(Carbonyl-methoxy polyethylene glycol-2000)-1,2-distearoyl-sn-glycero-3-phosphoethanolamine (mPEG2000-DSPE), hydrogenated soy phosphatidylcholine (HSPC) and cholesterol were obtained from A.V.T. Pharmaceutical Co., Ltd. (Shanghai, China). 1,1′-Dioctadecyl-3,3,3′,3′-tetramethyl indo tricarbocyanine iodide (DiR) was purchased from American ATT Bioquest, Inc (CA, USA). Roswell Park Memorial Institute 1640 Medium, trypsin, RIPA Lysis Buffer and penicillin/streptomycin were purchased from Meilun Biotechnology Co., Ltd. (Dalian, China). Fetal bovine serum was the product of Gibco, Invitrogen Corp. (Carlsbad, USA). Mouse TNF-α and IL-10 ELISA kit was obtained from eBioscience (CA, USA). Anti-mouse Foxp3 antibody and Anti-mouse Vegf-C antibody were purchased from Santa Cruz Biotechnology, Inc. (CA, USA). Goat anti-rabbit secondary antibody, streptavidin peroxidase and DAB were purchased form Zhongshan Biotechnology Co., Ltd. (Beijing, China).

Cell culture and animals

Murine sarcoma S180 cell line and murine RAW264.7 macrophages were obtained from the Cell Bank of the Chinese Academy of Sciences (Shanghai, China), and maintained in RPMI 1640 Medium (Meilunbio) containing 10% FBS (Gibco) at 37 °C in a humidified atmosphere of 5% CO_2.

Male Kunming mice (aged 6–7 weeks; weighing 18–22 g) were purchased from the Laboratory Animal Center of Shenyang Pharmaceutical University (Shenyang, China). All animal care and experiments were conducted in accordance with the guidelines for the care and use of the Animal Welfare Committee of Shenyang Pharmaceutical University.

MTT assay of RAW264.7 cells and S180 cells to DOX

RAW264.7 cells and S180 cells were seeded into 96-well plates (5×10^3 cells well^{-1}) and treated with DOX solution at various concentrations for 48 h. MTT solution (5 mg mL^{-1}) was added to each well and incubated for an additional 4 h. At the end of the experiment, the medium was replaced with 100 µL of DMSO to dissolve the formazan crystals, and the absorbance was measured at 570 nm using in a microplate reader (Model 680, Bio-Rad, USA). The cell viability was calculated according to Eq. (1):

$$\text{Cell viability (\%)} = \frac{OD_{exp} - OD_{blank}}{OD_{control} - OD_{blank}} \times 100\%, \quad (1)$$

OD_{exp} is the absorbance of the experimental group, OD_{blank} is the absorbance of the blank group, and $OD_{control}$ is the absorbance of the control group.

Preparation of DOX-RAW264.7 cells

Selection of DOX-loading time

DOX-loaded RAW264.7 cells were obtained by incubating RAW264.7 cells with DOX solution. The appropriate drug-loading time was confirmed based on cell uptake. Briefly, the RAW264.7 cells were lifted by scraping, washed by PBS, and then counted (5×10^5 cells mL^{-1}, 2.0 mL). After centrifuging at 1500 rpm for 5 min, the RAW264.7 cells were re-suspended in 2.0 mL DOX solution (PBS, 50 µg mL^{-1} DOX). Then the cell suspensions were cultured at 37 °C in a humidified atmosphere of 5% CO_2 for 0, 0.5, 1, 2 and 4 h. The cells were harvested and washed with PBS twice. Finally, the cellular uptake of DOX at different times (0, 0.5, 1, 2, and 4 h) was evaluated with a Quanta SC Flow cytometer (Beckman Coulter, CA, USA).

The status of DOX-loaded RAW264.7 cells

The status of the RAW264.7 cells at different DOX-loading time was evaluated by Laser Confocal Microscopy (ZEISS LSM 800, Germany). Briefly, RAW264.7 cells were seeded into nine-well plate chambered cover glass (2×10^5 cells per well) and incubated with DOX solution for 0.5, 1, 2 or 4 h. The cells were washed on the cover slips with PBS and DAPI solution was added to stain the nuclei for 15 min. Finally, the samples were observed and photographed using confocal microscopy.

The survival time of DOX-RAW264.7 cells

The cell survival time of DOX-RAW264.7 cells was determined by CCK-8 assay. RAW264.7 cells were seeded in 96-well plates (5×10^3 cells per well) and incubated with DOX (50 μg mL^{-1}) for 2 h. The medium was discarded and the cells were washed by PBS for three times. The cells were re-suspended with fresh media and cultured for 2, 4, 8, 12 and 24 h. The cells were observed under optical microscopy. Finally, CCK-8 solution (20 μL $well^{-1}$) was added and incubated for an additional 30 min. The absorbance of the formazan solution was measured at 450 nm in a microplate reader (Model 680, Bio-Rad, USA). The cell viability was calculated according to Eq. (1) as well.

Determination of TNF-α and IL-10 in RAW264.7 cells

The levels of cytokines (i.e., TNF-α and IL-10) in culture fluid of RAW264.7 cells before and after doxorubicin loading were determined using an ELISA kit and following the instructions provided by the manufacturer.

The DOX-loading capacity and drug release

To determine the DOX-loading capacity of RAW264.7 cells, we measured the amount of doxorubicin in DOX-RAW264.7 cells. Briefly, 1 million RAW264.7 cells were counted and incubated with doxorubicin for 2 h as before. Those DOX-RAW264.7 cells were washed with PBS for three times. After centrifugation, DOX-RAW264.7 cells were re-suspended and destructed by RIPA Lysis Buffer. Centrifuge again and transfer 200 μL supernatant to 96-well plates. The amount of doxorubicin was quantified by Microplate Reader at EX 480 nm, EM 590 nm fluorescence. The experiment was carried out three times.

The drug release behavior was investigated subsequently. As before, DOX-RAW264.7 cells were prepared and separated from the DOX solution by centrifugation and then re-suspended in 1.0 mL PBS. The tube containing the cells was placed in a 37 °C swing bed at 80 rpm. At 0 h, 1 h, 2 h, 4 h, 8 h, 12 h and 24 h, cellular samples were centrifuged. The amount of DOX in the media and intracellular part was determined by Microplate Reader and the percentage of DOX release/residue was calculated. Each time point was executed with three parallel samples.

Bio-distribution of RAW264.7 cells in S180 tumor-bearing mice

RAW 264.7 cells were labeled with DiR. Briefly, RAW264.7 cells (1×10^6) were incubated with DiR solution (0.3 mg mL^{-1}) in 37 °C with 5% CO_2 for 30 min. Next, the cell suspensions were centrifuged at 1200 rpm for 5 min to remove the media, and the residual cells were washed three times with PBS and diluted to 1×10^6 cells mL^{-1} for injection.

S180 cells (2×10^6 cells) were implanted into the right axillary flank of male Kunming mice (about 20 g) to establish mouse sarcoma model. When the tumor size reached around 200–300 mm^3, the mice were intravenously injected with free DiR solution (1 mg kg^{-1}) or DiR-labeled RAW264.7 cells (5×10^5 cells/mouse, equivalent to 1 mg kg^{-1} DiR). The in vivo fluorescence images were recorded at 1, 4, 8, and 12 h using a Kodak in vivo imaging system FX PRO (Bruker, Inc., USA) with excitation and emission bandpass filters centered at 720 nm and 790 nm, respectively. At the end of the experiment, tumors and major organs (heart, liver, spleen, lung, and kidney) were removed for fluorescent imaging. The mean fluorescence intensities (%) of tumors and different organs were calculated using a region of interest (ROI) analysis system.

The effect of DOX-loaded RAW264.7 cells on the S180 tumor-bearing mice

Male Kunming mice were subcutaneously injected with S180 cells (2×10^6 cells per mouse) in the right axillary flank on day 1. When tumor volumes reached 100 mm^3, the mice were randomly divided into three groups (6 per group) and intravenously injected with DOX-loaded RAW264.7 cells (1×10^5 cells per mouse equivalent to 20 μg DOX), DOX solution (20 μg), or an equal volume PBS on days 4, 7 and 10. At day 14, the mice were sacrificed and the level of TNF-α and IL-10 in blood serum was determined. The tumors and hearts were removed for pathological section (Hematoxylin–Eosin staining).

Throughout the trial, the mice were weighed every other day and the tumor size was measured with an electronic vernier caliper. The estimated volume was calculated according to Eq. (2). The area under tumor growth curve (AUTGC) was calculated by Origin 9 software. The Tumor-Inhibition (TI) Index was calculated according to Eq. (3), as a comprehensive parameter for evaluating both antitumor effect and toxicity [27]. The tumor density is assumed to be 1 g cm^{-3}

for the calculation of net body weight. The net change in body weight in tumor-bearing animals was used as a marker for toxicity, which could more reliably reflect the life quality of tumor-bearing mice.

$$\text{Tumor volume } (\text{mm}^3) = 0.5 \times a \times b^2, \quad (2)$$

$$\text{TI index} = \frac{\text{Body weight (g)}}{\text{Tumor weight (g)}}, \quad (3)$$

where "*a*" is the largest and "*b*" is the smallest diameter of tumor. $AUTGC_{exp}$ is the area under tumor growth curve of the experimental group; the $AUTGC_{control}$ is the area under tumor growth curve of the control group.

Preparation of Rapamycin-pegylated liposome

Rapamycin-pegylated liposome (RPPA-PL) was prepared using the reverse ethanol injection method. Briefly, the lipid mixture composed of HSPC/Cholesterol/mPEG2000-DSPE/Rapamycin (50.0/16.7/16.7/1.0, w/w) was dissolved in ethanol and evaporated at 65 °C to near-dryness. The resulting lipid film was hydrated with sterile water at 65 °C for 20 min with stirring. After hydration, the dispersion was sonicated using a laboratory ultrasonic cell pulverizer (JY92-II, Ningbo Scientz Biotechnology Co., Ltd., China), for a 2 min cycle (200 w) followed by an additional 4 min cycle (400 w). The liposomal solution was filtered through membranes for a uniform preparation. The rapamycin concentration was determined using the Agilent 1260 HPLC system with the Agilent C18 column (200 mm × 4.6 mm, 5 μm), operating at 278 nm. The mobile phase was methanol:water 80:20 (v/v), at a flow rate of 1 mL min^{-1} at 45 °C.

Preparation of inactivated RAW264.7 cells

The RAW 264.7 cells were collected by centrifuging, washed with PBS and then counted. One million cells were re-suspended and inactivated with 2 mL 4% paraformaldehyde for 2 h. The inactivated cells were washed with PBS, observed under microscope and then prepared for administration.

The effect of frequency, dose and viability of RAW264.7 cells on S180 tumor growth

Further animal experiments were carried out to determine the influence of frequency, dose and viability of RAW264.7 cells injected on the growth of S180 tumors. The S180 mouse sarcoma model was established as previous and divided into eight groups with six mice per group (Control group, RAPA-PL group, Groups 1–6). The dosage regimens of each group are presented in Table 1. Body weight and tumor size of mice were recorded as before.

Immunohistochemistry analysis

Male Kunming mice were subcutaneously injected with 2×10^6 S180 cells in the right axillary flank on day 1. The mice were randomly divided into three groups with three mice per group (Control, RAPA-PL, RAW264.7) and, respectively, injected with PBS, RAPA-PL (50 μg rapamycin per mouse), and RAW264.7 cells (1×10^5 cells per mouse) at days 4, 7, and 10. The mice were sacrificed at day 14 and the tumors, spleens and thymuses were removed for immunohistochemistry analysis.

Foxp3 and Vegf-C expression in each of the specimens was detected by immunohistochemistry using anti-Foxp3 antibody (Santa Cruz, USA, 1:100) and anti-Vegf-C antibody (Santa Cruz, USA, 1:100). The sections were deparaffinized in xylene, and rehydrated through graded alcohol and deionized water. For antigen retrieval, the sections were heated in a microwave oven in 0.3% citrate buffer (pH 6.0) for 5 min and washed with phosphate-buffered saline (PBS) three times for 5 min. Endogenous peroxidases were inactivated by a 25-min incubation in methanol-containing 3% H_2O_2, followed by three PBS washes for 5 min each. The slides were immune-stained with anti-Foxp3 antibody or anti-Vegf-C antibody at 4 °C overnight. Next, the slides were washed three times in PBS and exposed to goat anti-rabbit secondary antibody for 20 min, followed by treatment with streptavidin peroxidase. For color development, the slides were stained with DAB and then counterstained with hematoxylin followed by a wash with ammonia water. A brown

Table 1 Dosage regimens of each group

Group	Injection dose of RAW264.7 cells per mouse	Injection times
1	1×10^5 cells	1 (Day 4)
2	1×10^5 cells	2 (Day 4,7)
3	1×10^5 cells	3 (Day 4,7,10)
4	1×10^5 inactivated cells	3 (Day 4,7,10)
5	5×10^4 cells	3 (Day 4,7,10)
6	1×10^4 cells	3 (Day 4,7,10)
RAPA-PL	None (RAPA-PL as 50 μg rapamycin per mouse)	3 (Day 4,7,10)
Control	None (equal volume of PBS)	3 (Day 4,7,10)

precipitate in cells is indicative of a positive reaction. All images were captured on a digital microscope and images were analyzed using Image pro plus 6.0 software.

Statistical analyses

Results are presented as mean ± standard deviation (SD). One-way ANOVA was used for statistical comparison. The survival analysis was performed by the Kaplan–Meier method with GraphPad Prism 6.0 software. Statistical significance was set at $^{*}P < 0.05$ and $^{**}P < 0.01$.

Results

The effect of DOX on RAW264.7 cells and S180 cells viabilities

To examine the effect of DOX on cell viability, we measured the viability of RAW264.7 and S180 cells by MTT assay following incubation with DOX for 48 h. Both RAW264.7 and S180 cells displayed dose-dependent survival inhibition when treated for 48 h with DOX (Fig. 1a). DOX decreased cell viability with an IC50 of 1.56 ± 0.28 μg mL^{-1} for RAW264.7 cells and 0.52 ± 0.07 μg mL^{-1} for S180 cells. Compared with S180 cells, RAW264.7 cells displayed a relative resistance to DOX treatment. This result indicates that RAW264.7 cells could be a promising cellular carrier for DOX delivery.

Determination of DOX-loading time for RAW264.7 Cells

According to the results of the cytotoxic assays, we choose a high DOX concentration (50 μg mL^{-1}) for drug loading into RAW264.7 cells. The cellular uptake of DOX at different time points was compared by flow cytometry. The uptake increased along with the prolongation of incubation time and reached a maximum at 2 h. A slight decrease in uptake was observed for longer incubation time (Fig. 1b). Corresponding to the results of flow cytometry analysis, the fluorescent images of the uptake of DOX in RAW264.7 cells showed a maximum fluorescence at 2 h and no difference with that at 4 h (Fig. 1c). Therefore, 2 h was selected as a preferred time for drug loading.

The survival time of DOX-RAW264.7 cells

To further examine the survival time of DOX-RAW264.7 cells, we evaluated the viability of them in different periods (2, 4, 8, 12, and 24 h) by CCK-8 assay. After ingestion for 2 h, the cells gradually tended towards apoptosis. More than 60% of the cells died within 8 h and the cell population was completely dead within 24 h (Fig. 1e). We recorded the gradual apoptosis process of DOX-RAW264.7 cells by optical microscope imaging as seen in Fig. 1d. DOX is a cell cycle-nonspecific cytotoxic drug that inhibits the synthesis of DNA and RNA [28]. As shown in Fig. 1c, the pink area in confocal microscope images presents an obvious nuclei-like shape which indicated that most of DOX was distributed in nucleus and that those cells could hardly proliferate.

The DOX-loading capacity and drug release

DOX-loading content per million RAW264.7 cells was determined to be 203.2, 198.5 and 197.1 μg, separately in three tests. Namely, about 20 μg DOX was able to be uploaded into 1×10^5 cells, which was sufficient for subsequent pharmacodynamics experiment. The drug release behavior was shown in Fig. 1f. With the increase of incubation time, the intracellular drug gradually released and reached saturation at 8 h. Combined with the results of DOX-RAW264.7 cells viability test in Fig. 1e, it was suggested that cellular apoptosis was the main cause for drug release.

The changes of cytokine levels in RAW264.7 cells after DOX loading

The levels of TNF-α and IL-10 were determined in RAW264.7 cells before and after DOX loading. As the results presented on Fig. 1g, h, neither of cytokines levels (TNF-α and IL-10) showed a significant variation before and after drug loading. This result implied the interference of cytokine changes caused by DOX loading on subsequent in vivo experiments could be excluded.

Bio-distribution of RAW264.7 cells in S180 tumor-bearing mice

To verify the bio-distribution of RAW264.7 cells in vivo, DiR-labeled-RAW264.7 cells or free DiR solution was injected intravenously into S180 tumor-bearing mice. The fluorescent signals of labeled cells or free dye were recorded at 1, 4, 8 and 12 h post-injection using an in vivo imaging system. According to the results presented in Fig. 2a, the injection of the DiR solution gradually increased the fluorescent signal in tumors from 1 to 8 h with a slight decline at 12 h. However, the fluorescent signal was barely detectable in tumors of mice injected with DiR-RAW264.7 cells, but accumulated in the livers of these mice. The higher fluorescent intensity in the livers of mice treated with DiR-RAW264.7 cells suggested allo-recognition and elimination of RAW264.7 cells by recipient immune system.

The bio-distribution of RAW264.7 cells in major organs was assessed 12 h after injection. Compared with the DiR-RAW264.7 groups, the injection of free DiR solution led

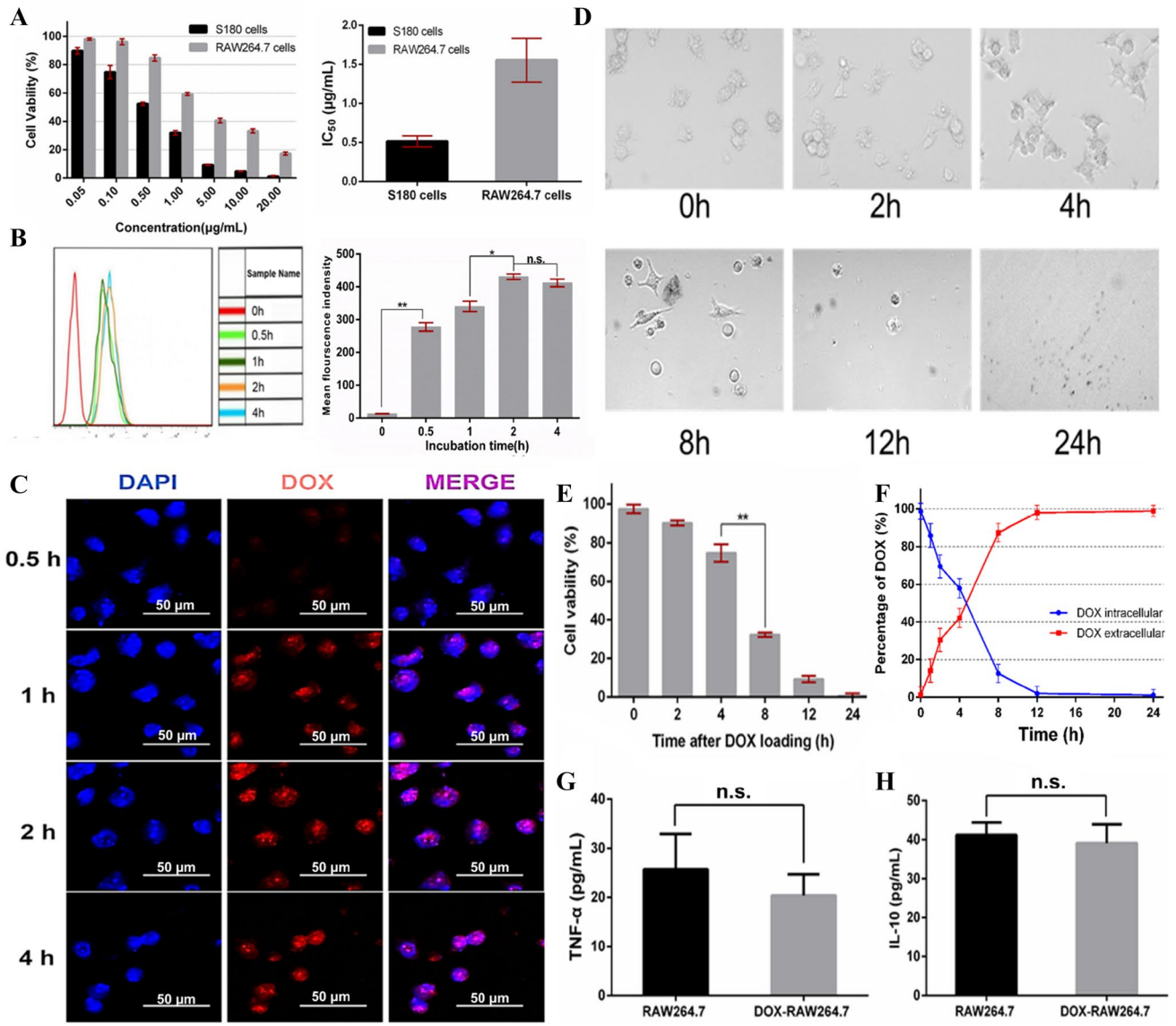

Fig. 1 **a** Cytotoxic effects of DOX on S180 and RAW264.7 cells. Cell viability was measured by MTT assay after exposure to DOX at different concentrations. **b** The uptake of DOX in RAW264.7 cells treated with 50 μg mL^{-1} DOX at different time. **c** Fluorescent images of DOX-loaded RAW264.7 cells with different loading time (scale bar 50 μm). **d** The morphology of DOX-RAW264.7 cells under optical microscope. **e** The cell viability of DOX-RAW264.7 cells after treatment with 50 μg mL^{-1} DOX for at different times. **f** The drug release extracellular (red) and drug residue intracellular (blue) of DOX-RAW264.7. **g** The levels of TNF-α in RAW264.7 and DOX-RAW264.7 cells. **h** The levels of IL-10 in RAW264.7 and DOX-RAW264.7 cells. Data shown are mean ± SD ($n = 6$) (*$P < 0.05$, **$P < 0.01$, no significant difference was marked as n.s.)

to a higher fluorescent signal in the lung due to its cationic charge [29]. In contrast, mice injected with DiR-RAW264.7 cells presented significantly elevated fluorescent signals in the liver, spleen and thymus ($P < 0.05$, Fig. 2b, c). This undesirable accumulation in immune organs indicated an acute transplant rejection following allogenic RAW264.7 cells injection. In addition, the accumulation of donor antigens in immune organs, especially in the thymus, could result in a long duration of interaction with the host immune system, thus, leading to immune tolerance.

Accelerated tumor growth phenomenon of DOX-RAW264.7 cells injection

To evaluate the biological effects of DOX-RAW264.7 cells in vivo, we employed a S180 sarcoma model in Kunming mice. The control group showed TI index of 6.57 ± 2.12, DOX group showed TI index of 18.95 ± 5.68. Surprisingly, the injection of DOX-RAW264.7 cells or RAW264.7 cells showed no antitumor effects, but accelerated tumor proliferation. As seen in Fig. 3a, the tumor

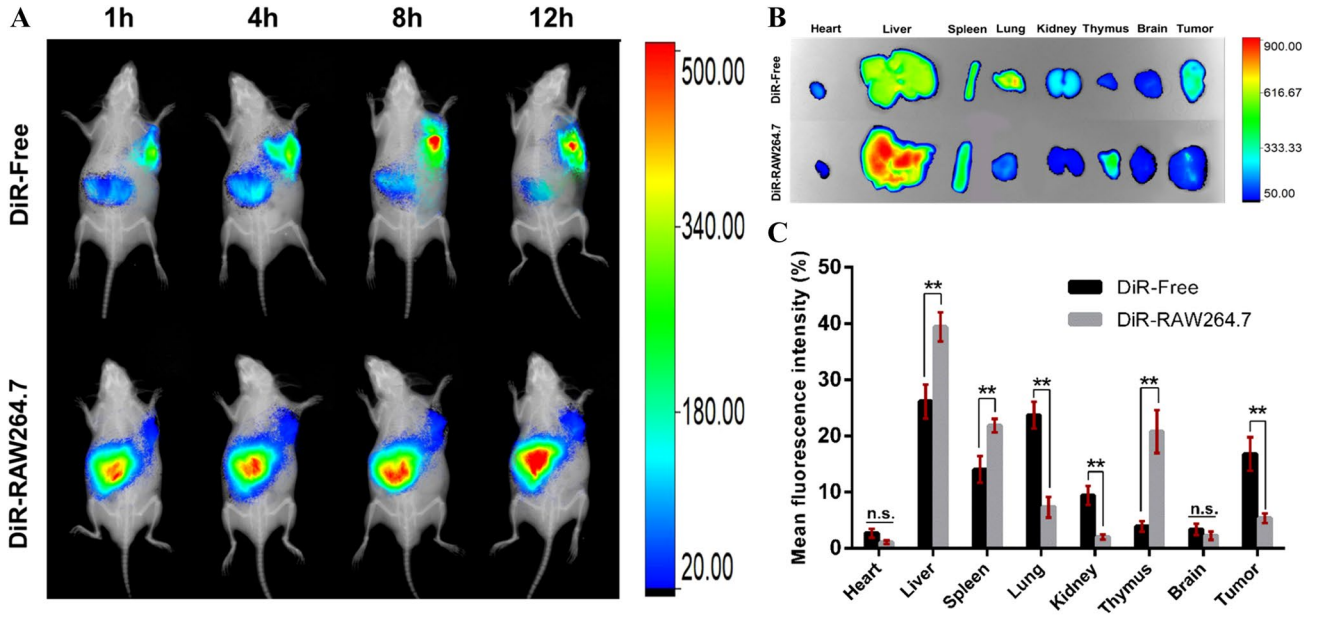

Fig. 2 In vivo bio-distribution of RAW264.7 cells in tumor-bearing mice. Tumor-bearing mice were intravenously injected with free DiR solution (1 mg kg^{-1}) or DiR-labeled RAW264.7 cells (5×10^5 cells/mouse, equivalent to 1 mg kg^{-1} DiR). **a** In vivo images of mice. **b** Fluorescence signals of excised tumors and organs at 12 h. **c** Mean fluorescent intensity of tumors and organs. Data shown are mean ± SD ($n = 3$) (**$P < 0.01$, no significant difference was marked as n.s.)

size in cellular injection group began to differ at day 12 ($P < 0.01$), and tumor growth was accelerated in DOX-RAW264.7 and RAW264.7 cells group. At the end of the experiment (day 14), the tumor volume of mice injected with DOX-RAW264.7 or RAW264.7 cells were enlarged nearly twice and three times compared with control group ($P < 0.01$), respectively.

Through the analysis of net body weight (Fig. 3b), the DOX-S group showed some toxicity but there was no significant difference between the DOX-RAW264.7, RAW264.7 cells and control groups ($P > 0.05$). In Fig. 3e, tissue sections showed that DOX-RAW264.7 did not inhibit tumor growth effectively. Interestingly, it was observed that all of the overgrown S180 tumors were intact and showed no obvious necrotic ulceration as the tumors in the control group (Fig. 3f). The serum cytokine levels (TNF-α and IL-10) were measured and presented on Fig. 3c, d. Compared with the control group, the TNF-α level of all the experimental groups was significantly lower ($P < 0.01$). A higher IL-10 level was detected in the mice injected with RAW264.7 or DOX-RAW264.7 cells ($P < 0.01$), which implied the immunosuppressive effects of mice in vivo. Based on this suggestive appearance, we suspected that the allogenic RAW264.7 cells, whether or not DOX loading, tolerated host immune and diminished its favorable immune response to the S180 tumor.

The effect of injection frequency, dose and viability of RAW264.7 cells on tumor growth

Groups with different injected frequencies (Group 1, 2, 3) and dose (Group 3, 5, 6) of RAW264.7 cells were designed to further explore whether the accelerated tumor growth phenomenon was dose or frequency dependent. We also set up the inactivated RAW264.7 cell group (Group 4) to validate the interference of cellular viability (as seen in Fig. 4c). To prove the correlation of immune tolerance and tumor overgrowth, we set up RAPA-PL group, using rapamycin to induce immune tolerance (RAPA-PL was shown in Fig. 4b). The tumor growth process in each group was captured by photography as shown in Fig. 4d.

The impact of the frequency of cell injection on tumor growth was presented in Fig. 5a. It was found that the growth of tumors in mice injected with 1×10^5 RAW264.7 cells for 1, 2, 3 times were significantly accelerated ($P < 0.01$). This result indicated that accelerated tumor growth could be induced by a single overdose injection.

The impact of cell injection quantity on tumor growth was presented in Fig. 5b. Similar to previous results, the mice in Group 3 and 5 displayed a trend of accelerated tumor growth starting around day 12. The tumor growth of mice injected with RAPA-PL showed a significant increase compared with the control group at day 14. However, when the cell quantity decreased to 1×10^4 cells per mouse

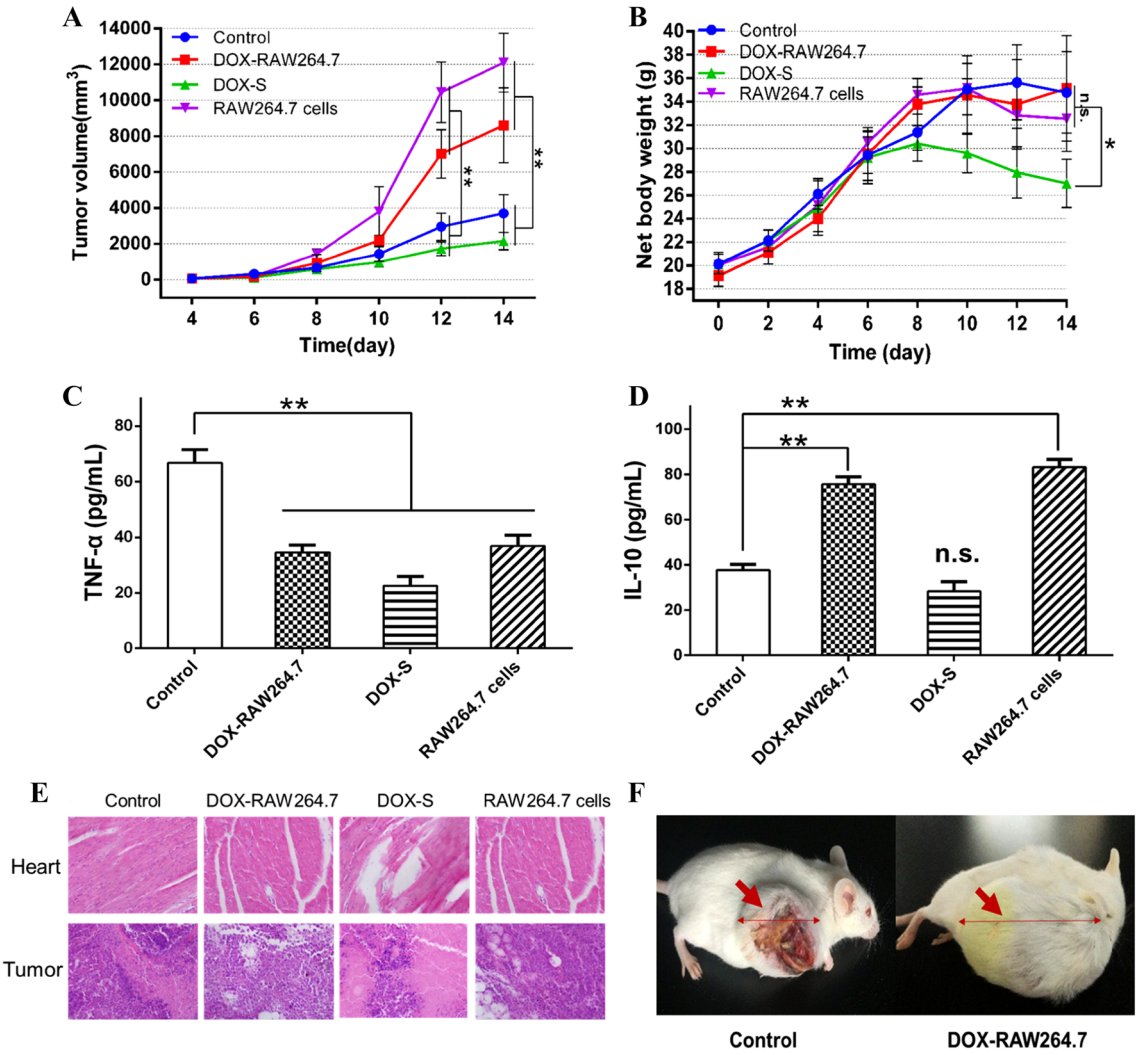

Fig. 3 Effect of DOX-loaded RAW264.7 cells on S180-tumor-bearing mice. **a** Tumor growth curve of mice treated with PBS, DOX-RAW264.7 (1×10^5 cells per mouse equivalent to 20 μg DOX), DOX (20 μg per mouse) and RAW264.7 cells (1×10^5 cells per mouse). **b** Net body weight change in tumor-bearing mice. **c** The levels of serum TNF-α of tumor-bearing mice. **d** The levels of serum IL-10 of tumor-bearing mice. **e** Histopathology of heart and tumor sections with hematoxylin and eosin (H&E) staining of different experimental groups (magnification × 200). **f** The appearance of ulcerated tumor (Control) and accelerated growth tumor (DOX-RAW264.7). Data are shown as mean ± SD ($n=6$) (*$P<0.05$, **$P<0.01$, no significant difference was marked as n.s.)

(Group 6), no tumor overgrowth was detected. These data suggested that a dose of allogenic cells of 1×10^4 cells per mouse could be disposed of by the mouse immune system without any obvious immune regulation. The accelerated tumor growth phenomenon was dose-dependent with the injection of RAW264.7 cells.

In addition, this accelerated tumor growth phenomenon was found in Group 4 as well. No significant difference was seen in tumor growth between the mice injected with inactivated RAW264.7 cells and those receiving living RAW264.7 cells ($P>0.05$, Fig. 5c). These results suggest that the acceleration of tumor growth is not due to the accumulation and proliferation of RAW264.7 cells in the tumor, but the immune tolerance induced by excessive antigen of RAW264.7.

The net body weight change is shown in Fig. 5d. No significant difference was detected between each experimental group and control group.

Determination of immune tolerance status

To confirm that immune tolerance was induced by allogenic RAW264.7 cells injection, it was important to determine the expression of relevant immune tolerance markers. We assessed the expression of Foxp3 and Vegf-C in the

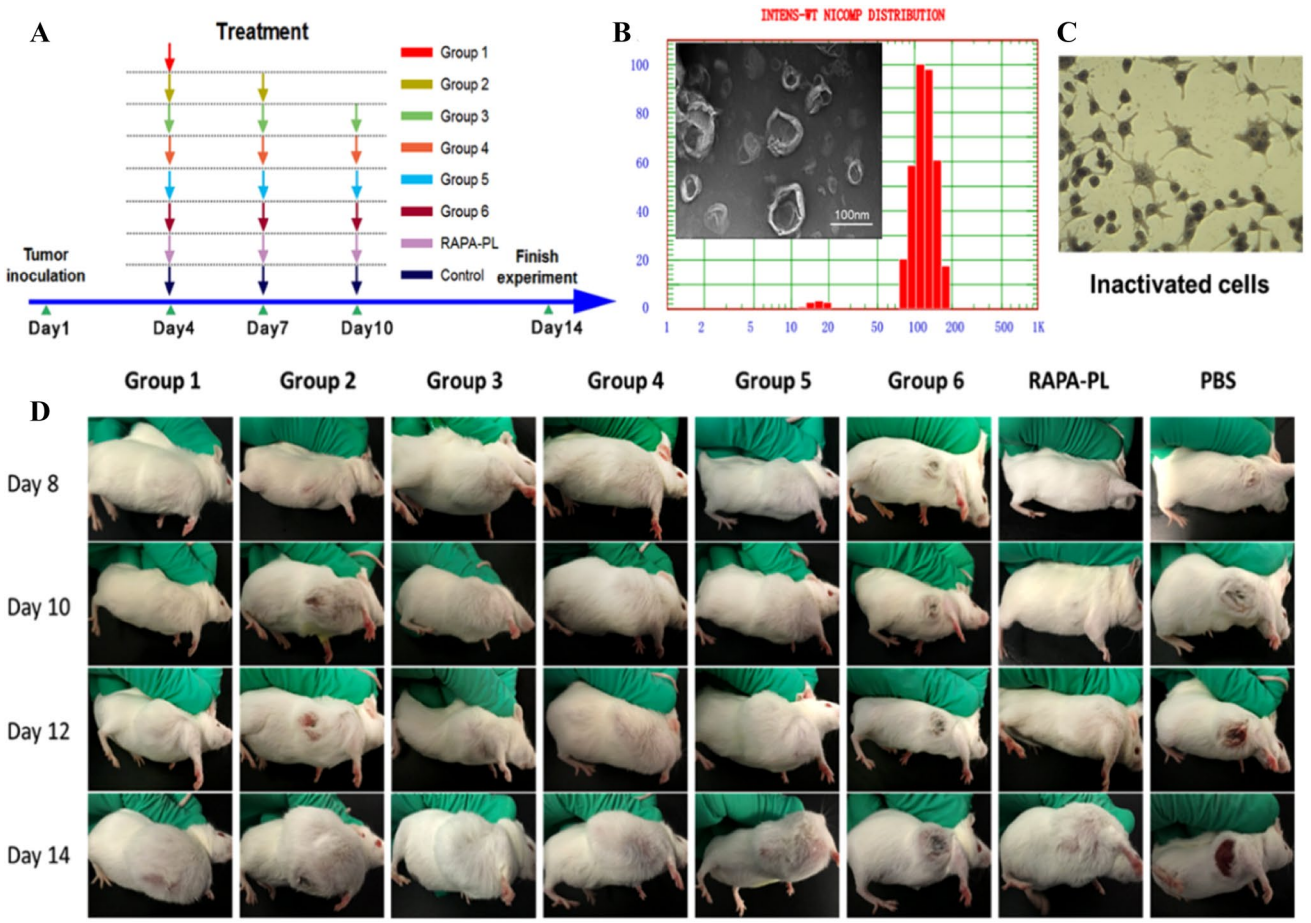

Fig. 4 **a** Representation of the treatment protocol applied to S180-bearing mice. **b** The particle size distribution and transmission electron microscope (TEM) image of RAPA-PL. **c** The morphology of inactivated RAW264.7 cells. **d** The process of tumor growth in each group

tumors, spleens and thymuses of mice injected with either PBS, RAPA-PL, or RAW264.7 cells. As demonstrated in Fig. 6a, b, the expression of Foxp3, the critical marker for T_{reg} cells [30], significantly increased in tumors and spleens of mice injected with RAPA-PL and RAW264.7 cells ($P < 0.01$). This result suggests that the injection of RAW264.7 cells generates T_{reg} cells in implanted tumor and lymphoid organs. As seen in Fig. 6c, d, the injection of RAPA-PL and RAW264.7 cells also resulted in the increased expression of Vegf-C in the tumors and spleens. No differences of Vegf-C expression were observed in the thymus between the groups. Compared to the RAPA-PL group, mice injected with RAW264.7 cells showed higher expression of Vegf-C in tumors. These results suggest that up-regulation of Vegf-C by RAW264.7 cells mediates peripheral lymphatic hyperplasia and dilation [31], directly promoting the S180 tumor invasion. Recent studies have revealed the critical role of Vegf-C in promoting immune tolerance and cross-presentation of tumor antigen [32].

Discussion

The published literatures about macrophage-mediated drug delivery system for cancer treatment was summarized in Table 2. Under the inspiration of Zhang Qiang's work [11], we have successfully constructed DOX-loaded RAW264.7 cells in vitro. In contrast to previous work, in our subsequent pharmacodynamics test, mice injected with DOX-RAW264.7 cells showed accelerated tumor growth unexpectedly. We confirmed that this phenomenon was cell dose-dependent and proposed that there was a critical value between 1×10^4 to 5×10^4 cells per mouse for the development of immune tolerance. We confirmed that the inactivated dead cells also promoted the tumor growth, suggesting that overgrowth was not directly related to the recruitment of live RAW264.7 cells but the antigens of the RAW264.7 cells. We observed an unusual thymus accumulation of RAW264.7 cells, which might be attributed to the migration of dendritic cells (DCs) [33, 34] that have captured DiR-labeled cell debris as presented antigen to

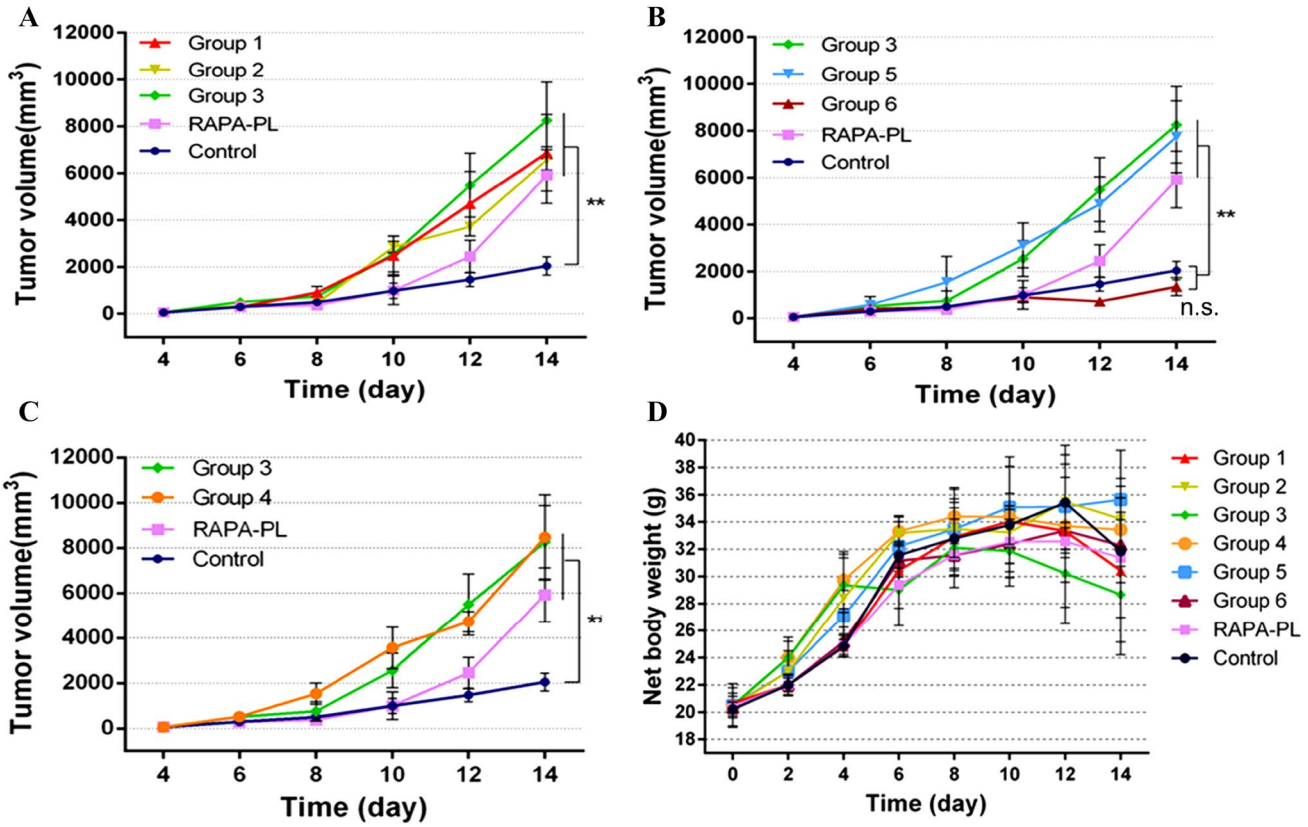

Fig. 5 Effect of injection frequency, dose, and viability of RAW264.7 cells on S180-tumor-bearing mice. **a** Impact of RAW264.7 cells injection frequency (Group 1: 1×10^5 cells injection once; Group 2: 1×10^5 cells injection twice; Group 3: 1×10^5 cells injection three times). **b** Impact of RAW264.7 cells injection quantity (Group 5: 5×10^4 cells injection three times; Group 6: 1×10^4 cells injection three times). **c** Impact of injection RAW264.7 cells activity (Group 4: 1×10^5 inactivated cells injection three times). **d** Net body weight change in tumor-bearing mice. Data are shown as mean ± SD ($n=6$) (*$P<0.05$, **$P<0.01$, no significant difference was marked as n.s.)

thymocytes. Further work was required to determine the underlying mechanism of thymus accumulation.

Rapamycin, an immunosuppressant used for transplantation, can induce T_{reg} activation in vivo and protect grafts from host immune rejection [39, 40]. We prepared RAPA-PL and confirmed its action in mediating immune tolerance. Interestingly, mice injected with RAPA-PL showed accelerated tumor growth, suggesting that this phenomenon was associated with immune tolerance. These findings are similar to the results of a study by Tien-Jen Lin et al. [41], who reported that rapamycin promoted mouse 4T1 tumor metastasis. Meanwhile, as indirect evidence, numerous clinical statistics have shown that patients who have long-term used immunosuppressive agents have a higher risk of cancer [42].

Tumor Necrosis Factor alpha (TNF-α) was a cytokine involved in systemic inflammation and was one of the cytokines that make up the acute phase reaction. It was produced chiefly by activated macrophages and able to induce fever, apoptotic cell death, inflammation and to inhibit tumorigenesis [43]. Interleukin-10 (IL-10) was an anti-inflammatory cytokine, which was well known for its immunosuppressive function. IL-10 acted on a variety of immune cell subsets and played an immunosuppressive effect through a variety of ways [44]. Before and after DOX loading, the TNF-α and IL-10 levels in RAW264.7 cells showed no significant change. However, the mice injected with DOX-RAW264.7 or RAW264.7 cells showed a distinctly higher IL-10 levels and lower TNF-α levels at day 14. It meant that these mice were in a state of immunosuppression. The mice treated with DOX solution also showed a lower TNF-α, which may be attributed to the toxicity of DOX to immune cells.

Despite the nude mice were widely used in cell-mediated drug delivery researches, their immunodeficiency intrinsically flawed in their value to predict the potential connections between transplanted cells, host immune system and tumor growth. Thus, we chose the S180-bearing mice, which possess a complete immune system, to evaluate the in vivo effect of allogenic RAW264.7 cells. The rapid growth and proliferation of S180 amplifies the signals of accelerating tumor growth under the host immune tolerance and make it measurable as 2–3 times tumor volume enlarged. Moreover,

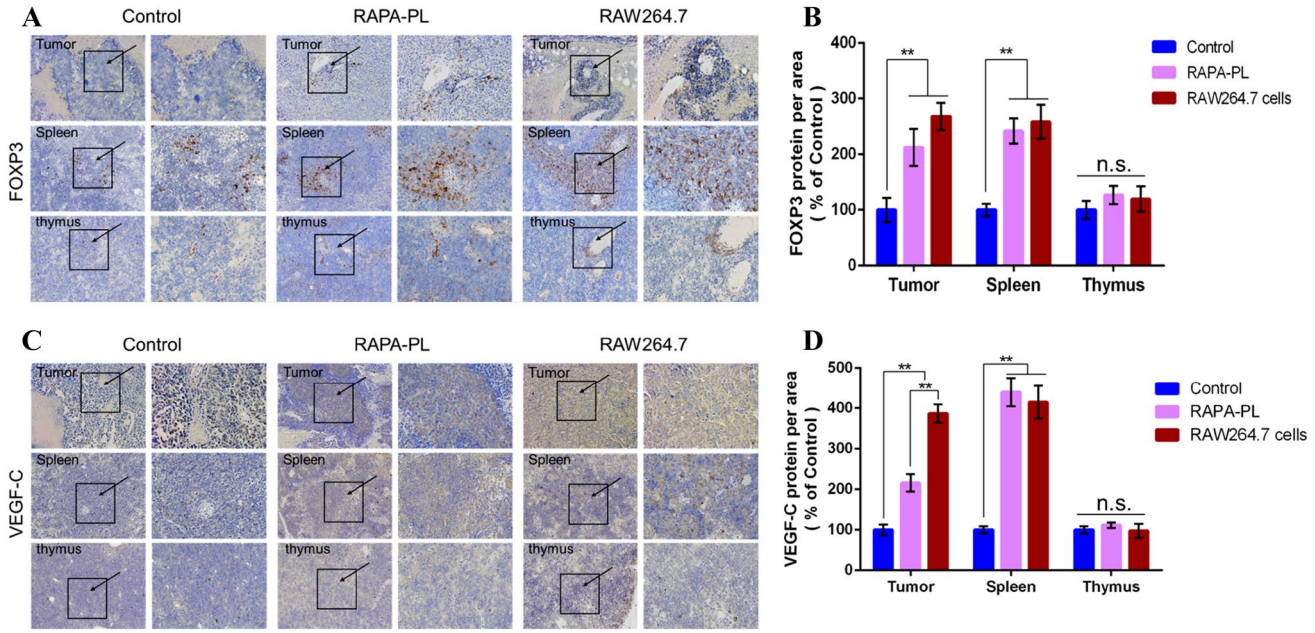

Fig. 6 Expression of Foxp3 (**a, b**) and Vegf-C (**c, d**) in tumor, spleen and thymus of S180 tumor-bearing mice treated with PBS (Control), RAPA-PL or RAW264.7 cells (magnification × 200 and × 400). Data are presented as the mean ± SD ($n = 3$) (**$P < 0.01$, no significant difference was marked as n.s.)

safety and efficacy studies of cell-mediated drug delivery based on immune complete mice were more valuable for its further clinical transformation.

Still, the possibility that the phenomenon described in the present study was dependent on the RAW264.7 cells could not be excluded. Further studies are needed to demonstrate whether this phenomenon also applies to other allogeneic cells. Even if RAW264.7 cells have the potential to deliver the therapeutic agent in the tumor, their antigenicity might limit the effect of this agent. It is important to consider that artificial reconstructions such as drug loading or genetically modified CAR-T might increase the immunogenicity of autologous cells leading to long-term immune tolerance. Based on our results, we predict that in situ programming of drug-loaded monocytes/macrophages or leukemia-specific T cells would be more immune-competent for tumor treatment. Indeed, this hypothesis was supported by some published experimental data [45, 46].

Conclusions

In summary, RAW264.7 cell possessed both the immunogenicity and pro-tumorigenic property, which made it unsuitable as allograft drug carrier. We reported an accelerated tumor growth phenomenon in S180 tumor-bearing mice followed with DOX-loaded RAW264.7 cells injection. This phenomenon was dose-dependent on the injected RAW264.7 cells and irrelevant to injection frequency or cellular viability. We confirmed that the induction of immune tolerance by the transfusion of allogeneic RAW264.7 cells was one of the main reasons for the accelerated tumor growth. In the process that allograft RAW264.7 cells were disposed as foreigners by the host immune system, these cells disturbed the immunologic balance and induced an immune tolerance accompanied with rapid tumor growth. Our study calls into question the suitability of RAW264.7 cell used in the cell-based drug delivery for cancer therapy and provides an experimental basis on safety studies of cell-mediated drug delivery systems for further clinical applications.

Table 2 The summary of published literatures about macrophage-mediated drug delivery system for cancer treatment

Cellular carrier	Model drug	Animal strain	Cancer model	Main results	References
Murine RAW264.7 macrophages	Free doxorubicin	Balb/c mice	Lung metastasis of breast cancer	DOX-loaded RAW264.7 cells showed promising anticancer efficacy in terms of tumor suppression, life span prolongation and metastasis inhibition, with reduced toxicity	[11]
	Doxorubicin-loaded PLGA nanoparticles	Balb/c nude mice	Glioma	Nanoparticle-loaded RAW264.7 cells reduced liver accumulation and increased brain distribution of the drug	[12]
	Doxorubicin-loaded gold nanorod/albumin	C57BL/6J mice	Prostatic cancer	Nanoparticle-loaded RAW264.7 cells improved photothermal/chemodrug distribution and retention ability to achieve enhanced antitumor effects	[13]
	Paramagnetic iron/iron oxide nanoparticles	C57BL/6 mice	Pancreatic cancer	Nanoparticle-loaded RAW264.7 cells significantly increased survival in a murine pancreatic cancer model	[35]
	Echogenic polymer/C_5F_{12} bubbles and doxorubicin-loaded polymer vesicles	C57BL/6JNarl mice	Prostatic cancer	RAW264.7 cell-mediated co-delivery of echogenic polymer bubbles and doxorubicin vesicles penetrated deeply within pre-irradiated tumor and improved chemotherapy	[36]
Rat NR8383 alveolar macrophages	Gold–silica nanoshells	Sprague Dawley rats	Glioma	Nanoshell-loaded alveolar macrophages prevented/delayed glioma development	[37]
Isolated mouse peritoneal macrophage	Liposomal doxorubicin	Balb/c nude mice	Lung tumor	Liposomal doxorubicin-loaded macrophages effectively inhibited subcutaneous and metastasis xenograft A549 tumor	[38]

Acknowledgements We would like to thank Experimental Animal Center of Shenyang Pharmaceutical University for their careful care to animals.

Funding This work was funded by the National Natural Science Foundation of China (nos. 81703456 and 81373334) and Science and technology Department of Liaoning Province (no. 201601140).

Compliance with ethical standards

Conflict of interest All authors declare that they have no conflicts of interest.

Ethical approval All procedures performed in studies involving animal experiments were in accordance with the ethical standards of the Animal Ethics Committee of Shenyang Pharmaceutical University. This article does not contain any studies with human participants performed by any of the authors.

References

1. Dou H, Destache CJ, Morehead JR, Mosley RL, Boska MD, Kingsley J et al (2006) Development of a macrophage-based nanoparticle platform for antiretroviral drug delivery. Blood 108:2827–2835
2. Klyachko NL, Polak R, Haney MJ, Zhao Y, Gomes Neto RJ, Hill MC et al (2017) Macrophages with cellular backpacks for targeted drug delivery to the brain. Biomaterials 140:79–87
3. Ye ZP, Ai XL, Faramand AM, Fang F (2018) Macrophages as nanocarriers for drug delivery: novel therapeutics for central nervous system diseases. J Nanosci Nanotechnol 18:471–485
4. Lewis CE, Pollard JW (2006) Distinct role of macrophages in different tumor microenvironments. Can Res 66:605–612
5. Sica A, Bronte V. Sica A, Bronte V (2007) Altered macrophage differentiation and immune dysfunction in tumor development. J Clin Invest 117:1155–1166
6. Mantovani A, Schioppa T, Porta C, Allavena P, Sica A (2006) Role of tumor-associated macrophages in tumor progression and invasion. Cancer Metastas Rev 25:315–322
7. Brennen N, Levy O, Han E, Rosen DM, Musabeyezu J, Safaee H et al (2016) Abstract 2067: attacking prostate cancer with a prodrug-doped cellular Trojan horse. Can Res 76:2067-
8. Choi MR, Stantonmaxey KJ, Stanley JK, Levin CS, Bardhan R, Akin D et al (2007) A cellular Trojan horse for delivery of therapeutic nanoparticles into tumors. Nano Lett 7:3759–3765
9. Batrakova EV, Gendelman HE, Kabanov AV (2011) Cell-mediated drug delivery. Expert Opin Drug Deliv 8:415
10. Brynskikh AM, Zhao Y, Mosley RL, Li S, Boska MD, Klyachko NL et al (2010) Macrophage delivery of therapeutic nanozymes in a murine model of Parkinson's Disease. Nanomedicine Nanotechnol Biol Med 5:379–396
11. Fu J, Wang D, Mei D, Zhang H, Wang Z, He B et al (2015) Macrophage mediated biomimetic delivery system for the treatment of lung metastasis of breast cancer. J Control Release 204:11–19
12. Pang L, Qin J, Han L, Zhao W, Liang J, Xie Z et al (2016) Exploiting macrophages as targeted carrier to guide nanoparticles into glioma. Oncotarget 7:37081–37091
13. Chiu HT, Su CK, Sun YC, Chiang CS, Huang YF (2017) Albumin–gold nanorod nanoplatform for cell-mediated tumoritropic delivery with homogenous chemodrug distribution and enhanced retention ability. Theranostics 7:3034–3052
14. Zhao Y, Haney MJ, Gupta R, Bohnsack JP, He Z, Kabanov AV et al (2014) GDNF-transfected macrophages produce potent neuroprotective effects in Parkinson's disease mouse model. PLoS One 9:e106867
15. Raschke WC, Baird S, Ralph P, Nakoinz I (1978) Functional macrophage cell lines transformed by Abelson leukemia virus. Cell 15:261–267
16. Harris AC, Ferrara JLM, Levine JE (2013) Advances in predicting acute GVHD. Br J Haematol 160:288–302
17. Defrancesco L (2014) CAR-T cell therapy seeks strategies to harness cytokine storm. Nat Biotechnol 32:604
18. Lee DW, Gardner R, Porter DL, Louis CU, Ahmed N, Jensen M et al (2016) Current concepts in the diagnosis and management of cytokine release syndrome. Blood 124:188–195
19. Leventhal J, Abecassis M, Miller J, Gallon L, Ravindra K, Tollerud DJ et al (2012) Chimerism and tolerance without GVHD or engraftment syndrome in HLA-mismatched combined kidney and hematopoietic stem cell transplantation. Sci Transl Med 4:124ra28
20. Scandling JD, Busque S, Dejbakhshjones S, Benike C, Millan MT, Shizuru JA et al (2008) Tolerance and chimerism after renal and hematopoietic-cell transplantation. N Engl J Med 358:362–368
21. Roncarolo MG, Battaglia M (2007) Regulatory T-cell immunotherapy for tolerance to self antigens and alloantigens in humans. Nat Rev Immunol 7:585–598
22. Wood KJ, Bushell A, Hester J (2012) Regulatory immune cells in transplantation. Nat Rev Immunol 12:417–430
23. Chen DS, Mellman I (2013) Oncology meets immunology: the cancer-immunity cycle. Immunity 39:1–10
24. de Visser KE, Eichten A, Coussens LM (2006) Paradoxical roles of the immune system during cancer development. Nat Rev Cancer 6:24–37
25. Fung JJ, Jain A, Kwak EJ, Kusne S, Dvorchik I, Eghtesad B (2001) De novo malignancies after liver transplantation: a major cause of late death. Liver Transpl 7:S109
26. Curiel TJ, Coukos G, Zou L, Alvarez X, Cheng P, Mottram P et al (2004) Specific recruitment of regulatory T cells in ovarian carcinoma fosters immune privilege and predicts reduced survival. Nat Med 10:942–949
27. Xiang Luo LH, Zheng H, Liu M, Liu X, Li C, Qiu Q, Zhao Z, Cheng X, Lai C, Yuqing S, Yihui D, Yanzhi S (2018) Neutrophil-mediated delivery of pixantrone-loaded liposomes decorated with poly(sialic acid)–octadecylamine conjugate for lung cancer treatment. Drug Deliv 25(1):1200–1212
28. Fan H, Li H, Liu G, Cong W, Zhao H, Cao W et al (2017) Doxorubicin combined with low intensity ultrasound suppresses the growth of oral squamous cell carcinoma in culture and in xenografts. J Exp Clin Cancer Res 36:163
29. Verbaan FJ, Oussoren C, Dam IMV, Takakura Y, Hashida M, Crommelin DJA et al (2001) The fate of poly(2-dimethyl amino ethyl)methacrylate-based polyplexes after intravenous administration. Int J Pharm 214:99–101
30. Hori S, Nomura T, Sakaguchi S (2003) Control of regulatory T cell development by the transcription factor Foxp3. Science 299(5609):1057–1061
31. Tammela T, Alitalo K (2010) Lymphangiogenesis: molecular mechanisms and future promise. Cell 140:460–476
32. Lund AW, Duraes FV, Hirosue S, Raghavan VR, Nembrini C, Thomas SN et al (2012) VEGF-C promotes immune tolerance in B16 melanomas and cross-presentation of tumor antigen by lymph node lymphatics. Cell Rep 1:191
33. Bonasio R, Scimone ML, Schaerli P, Grabie N, Lichtman AH, von Andrian UH (2006) Clonal deletion of thymocytes by circulating dendritic cells homing to the thymus. Nat Immunol 7:1092

34. Hadeiba H, Lahl K, Edalati A, Oderup C, Habtezion A, Pachynski R et al (2012) Plasmacytoid dendritic cells transport peripheral antigens to the thymus to promote central tolerance. Immunity 36:438–450
35. Basel MT, Balivada S, Wang H, Shrestha TB, Seo GM, Pyle M et al (2012) Cell-delivered magnetic nanoparticles caused hyperthermia-mediated increased survival in a murine pancreatic cancer model. Int J Nanomedicine 7:297–306
36. Huang WC, Chiang WH, Cheng YH, Lin WC, Yu CF, Yen CY et al (2015) Tumortropic monocyte-mediated delivery of echogenic polymer bubbles and therapeutic vesicles for chemotherapy of tumor hypoxia. Biomaterials 71:71–83
37. Madsen SJ, Christie C, Hong SJ, Trinidad A, Peng Q, Uzal FA et al (2015) Nanoparticle-loaded macrophage-mediated photothermal therapy: potential for glioma treatment. Lasers Med Sci 30:1357–1365
38. Choi J, Kim HY, Ju EJ, Jung J, Park J, Chung HK et al (2012) Use of macrophages to deliver therapeutic and imaging contrast agents to tumors. Biomaterials 33:4195–4203
39. Fischer R, Turnquist HR, Taner T, Thomson AW (2009) Use of rapamycin in the induction of tolerogenic dendritic cells. Handb Exp Pharmacol 188:215–232
40. Kishimoto TK, Ferrari JD, Lamothe RA, Kolte PN, Griset AP, O'Neil C et al (2016) Improving the efficacy and safety of biologic drugs with tolerogenic nanoparticles. Nat Nanotechnol 11:890
41. Lin TJ, Liang WM, Hsiao PW, Wei PMS, Lin WC (2015) HT, et al. Rapamycin promotes mouse 4T1 tumor metastasis that can be reversed by a dendritic cell-based vaccine. PLoS One 10:e0138335
42. Dantal J, Soulillou JP (2005) Immunosuppressive drugs and the risk of cancer after organ transplantation. N Engl J Med 352:1371–1373
43. Van HR, Ten Hagen TL, Eggermont AM (2006) TNF-alpha in cancer treatment: molecular insights, antitumor effects, and clinical utility. Oncologist 11:397–408
44. Saraiva M, O'Garra A (2010) The regulation of IL-10 production by immune cells. Nat Rev Immunol 10:170–181
45. Smith TT, Stephan SB, Moffett HF, Mcknight LE, Ji W, Reiman D et al (2017) In situ programming of leukaemia-specific T cells using synthetic DNA nanocarriers. Nat Nanotechnol 12:813
46. She Z, Zhang T, Wang X, Li X, Song Y, Cheng X et al (2014) The anticancer efficacy of pixantrone-loaded liposomes decorated with sialic acid–octadecylamine conjugate. Biomaterials 35:5216–5225